Conference Proceedings

EuroSun 2014
Aix-les-Bains (France), 16 - 19 September 2014

THERMAL PERFORMANCE ANALYSIS OF A CONCENTRATING BEAM SPLITTING HYBRID PVT COLLECTOR

Cameron Stanley[1], Ahmad Mojiri[1], Nitin Karwa[1] and Gary Rosengarten[1]

[1] RMIT University, Melbourne (Australia)

Summary

Typically the maximum fluid outlet temperature of a solar photovoltaic/thermal PVT collector is limited by the maximum operating temperature of the silicon PV cells. Spectral beam splitting has been demonstrated as a means of decoupling the thermal absorber from the PV cells, allowing thermal energy outputs in excess of the optimal PV cell operating temperatures. The current work describes the thermal performance analysis of a concentrating hybrid beam splitting PVT system designed to operate on linear concentrators and generate high-grade thermal output up to 150^{0}C together with a secondary low-grade thermal output at around 60^{0}C. Computational heat transfer simulations were conducted at various operating conditions in order to explore the heat loss and thermal efficiency of the hybrid receiver. PV cell temperatures were shown to remain below 75^{0}C under worst case scenarios. Hot stream thermal efficiencies of around 50% were demonstrated under typical ambient operating conditions. The effects of convective heat loss were shown to significantly degrade the thermal efficiency.

Key words: Hybrid PVT, Spectral beam splitting, Concentrating, Heat transfer, Modelling

1. Introduction

Silicon PV cells have typical electrical conversion efficiency in the range of 15-25%, with the balance of the incident solar energy either reflected or dissipated within the Silicon cells in the form of heat. Solar photovoltaic/thermal (PVT) collectors are capable of simultaneously generating electricity and thermal energy on the same collector. Typically thermal energy is extracted from the waste heat generated in the photovoltaic cell during the electrical conversion process.

In their simplest form PVT collectors consist of a fluid channel (air or water) flowing adjacent to the PV cell. Heat generated within the PV cell is transferred to the fluid and is carried away to be used for domestic hot water (eg. Chow et al. (2006),Dupeyrat et al. (2011)) or space heating (eg. Fraisse et al. (2007). In addition to absorbing heat which would otherwise be lost, the fluid also serves to lower the PV cell temperature. However the use of the fluid to cool the cells fundamentally conflicts with the desire to achieve high fluid temperatures, as the electrical conversion efficiency of the PV cells is negatively impacted with elevated temperatures.

Spectral beam splitting can be used to thermally decouple the fluid stream from the PV cells. In this approach the solar spectrum is decomposed into different spectral bands. The most suitable spectral band of light for photovoltaic conversion is directed to high efficiency silicon solar cells and the rest of the spectrum is absorbed as heat in a thermal receiver. By splitting the incident radiation in this way the solar cells and the thermal receiver can be thermally decoupled from each other. This allows the temperature of the thermal output to increase independently of the cell temperature e.g. the thermal output can be above 150^{o}C whereas the cell temperature is kept well below 80^{o}C.

A number of different techniques have been proposed to achieve spectral beam splitting including; selective absorption (Chendo et al., 1987) and wave interference filtering (Peters et al., 2010). The current work describes the thermal performance analysis of a novel hybrid beam splitting PVT collector which uses a volumetric absorption method to split the incident radiation.

Selection and/or peer review under responsibility of EuroSun2014 Scientific Committee
doi:10.18086/eurosun.2014.16.22 Available at http://proceedings.ises.org

2. Concentrating Hybrid PVT Design

A new design for a spectrally splitting PVT hybrid receiver for linear solar concentrators has been developed. This receiver can be optimised for both parabolic troughs and Fresnel concentrators, however the specific dimensions and thermal performance results presented in this paper apply to the receiver installed at the focal region of the NEP Solar Polytrough 1200, parabolic trough collector (see Tab. 1). A general schematic of the hybrid receiver is shown in Figure 1. Concentrated radiation is directed onto the base of the borosilicate glass thermal receiver tube. A heat transfer fluid (Propylene glycol) flowing within volumetrically absorbs the infrared band of the spectrum ($\lambda > 1100$nm) efficiently and transmits wavelengths below 1100nm. A 2mm thick, 25mm wide, coloured glass filter aligned horizontally across the middle of the thermal receiver tube acts as a high pass filter, absorbing wavelengths in UV-Vis range up to a desired cut-off wavelength (λ_1) and transmitting wavelengths longer than this value. The determination of the width of the filter was based on flux mapping measurements performed using a radiometry method developed by the authors on the 1.2m aperture width parabolic collector (Mojiri et al., 2014a). A slightly wider filter than the measured width of the flux distribution (≈ 22mm) was used to allow all light to be collected by the receiver in the presence of slight collector alignment errors. The energy absorbed in the liquid and the coloured glass filter, which then transfers into the liquid, raising its temperature independently of the cell temperature.

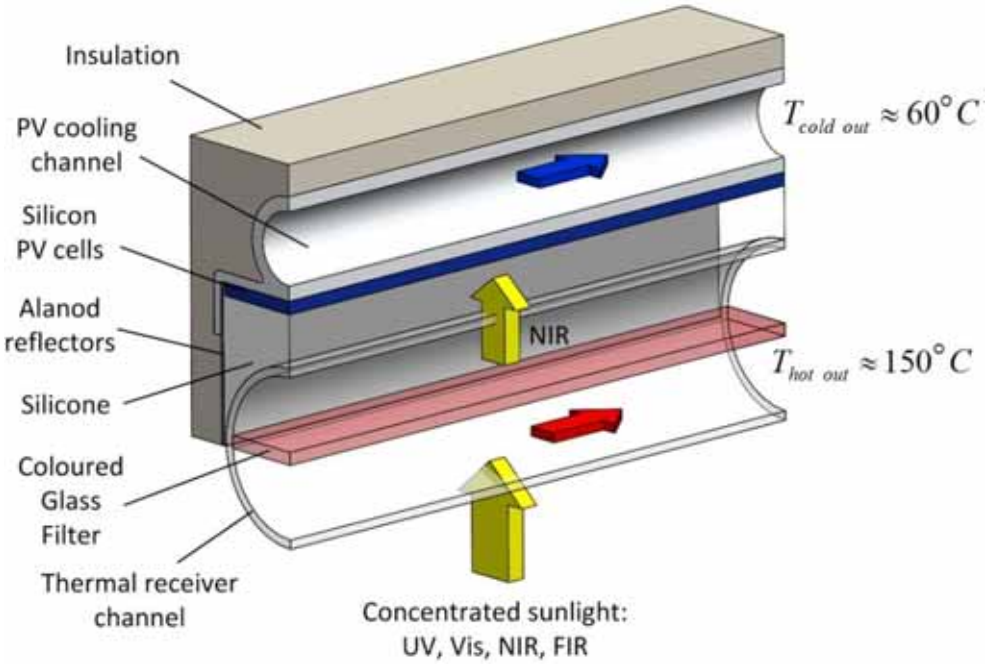

Fig. 1 General schematic of the hybrid beam splitting PVT collector

The remaining wavelengths, between λ_1 and 1100nm, are transmitted to the silicon cells, which are mounted into an aluminium extrusion with an integrated cooling channel. For light with wavelengths in this range the silicon cells exhibit improved electrical conversion efficiency (approx. 30%, with respect to the total solar energy available within this band) when compared to broad spectrum irradiance. The space between the thermal receiver tube and the silicon PV cells is filled with transparent silicone, which optically couples the cells with the borosilicate tube and limits reflective losses. In addition it also adds some thermal resistance between the tube and the silicon cells.

Thin alanod reflective sheets mounted to the internal wall of the aluminium extrusion and aligned parallel to the collector normal direct the light waves that are transmitted through the thermal receiver tube to the PV cells. A small gap (≈ 0.5mm) is maintained between the outer diameter of the absorber tube and the alanod mirrors in order to break the thermal conduction pathway, whilst minimising optical losses.

The receiver is designed with a nominal outlet temperature from the thermal receiver (hot stream) of 150^{o}C, with an outlet temperature of 60^{o}C from the secondary PV cell cooling channel. The high temperature output from the hybrid collector is intended to be coupled to a solar air conditioning system, while the low grade thermal output from the PV cooling channel can be either used for domestic hot water or as pre-heat for the hot fluid stream. This combination of outputs will create an efficient, building solar energy solution,

integrated into a single package.

3. Computational model and solution method

Numerical heat transfer modeling for a range of operating conditions was conducted using ANSYS CFX version 14.5. Structured quadrilateral mesh was used wherever the geometry permitted, with unstructured tetrahedral mesh elements used for regions with curvilinear shape. To dramatically reduce computational time and allow for many more operational points to be simulated both liquid streams within the hybrid receiver were not modeled. Instead, heat transfer between the fluid regions and the adjacent solids was modeled using convective heat transfer boundary conditions; both for the interior fluid channels, and the exterior ambient conditions (see section b below).

The fraction of thermal energy absorbed and transmitted by the various elements in the receiver were assumed from optical ray trace modeling presented by (Mojiri et al., 2014b). Tab. 1 presents a summary of the solar flux inputs to the various components of the receiver. Assuming a coloured filter with an ideal cut off frequency of λ_1 = 700nm, approximately 30% of the incident radiation was directed to the silicon PV cells, while the remaining 70% of the energy was absorbed within the thermal receiver. Two different values of direct normal radiation were considered: 650 W/m^2 and 900 W/m^2.

Tab. 1 Radiation flux inputs determined from optical ray trace modeling reported by Mojiri et al. (2014b)

Parameter	Quantity
Collector aperture	1.2 m
Collector length	2.0 m
Normal direct radiation	650 W/m^2, 900 W/m^2
Coloured filter cut-off frequency	700 nm
Total incident power	1560 W, 2160 W
Fraction of energy > 1100nm	25 % (390 W, 460 W)
Fraction of energy < 700nm	45 % (702 W, 972 W)
Fraction of energy 700 ≤ λ ≤ 1100nm	30 % (468 W, 648 W)
PV conversion efficiency	30 %
Electrical power output	9 % (140.4 W, 194.4 W)
Heat generated in PV Cell	21 % (327.6 W, 453.6 W)

A constant nominal thermal channel and cooling channel flow rate of 5 L/min and 2.5L/min respectively were used for all cases. It is expected that the thermal absorption within the beam splitting receiver will be complex. The boundary layer of the propylene glycol flowing adjacent to the front of the thermal absorber tube will volumetrically absorb the infrared wavelengths (λ > 1100nm). Also, the heat absorbed within the filter will be transferred to the fluid streams above and below the filter. This non uniform heat absorption is likely to result is a slightly higher heat addition to the flow beneath the filter than to the fluid stream above it.

A simplifying estimation of this complex flux situation is to assume that the total heat addition occurs uniformly throughout the fluid stream volumes. The filter and fluid streams can then be removed from the simulation. Instead, heat transfer between the fluid regions and the adjacent solids was modeled using convective heat transfer boundary conditions; both for the interior fluid channels, and the exterior ambient conditions. Variation in fluid properties with temperature were accounted for and adjustments to the Re and Nu were made accordingly.

An electrical conversion of 30% has been used for the silicon PV cells. The fraction of the solar flux transmitted to the PV cells which could not be converted to electricity was assumed to be dissipated as heat and modeled as a volumetric heat source in the computational model. Variations of the PV cell efficiency as a function of the PV cell temperature was not considered in the iterative solution procedure.

a. Iterative Solution Procedure

As the bulk mean fluid temperature, $T_f = (T_{in} + T_{out})/2$, was used as a convective heat transfer boundary condition, and the fluid outlet temperature, T_{out}, is a function of the heat transfer within the receiver, an iterative solution procedure was required.

The heat transfer coefficient for each stream was determined using the appropriate correlations (section b) at

the Reynolds number, *Re*, and Prandtl number calculated at the bulk mean fluid temperatures. For an initial approximation T_f was determined using an energy balance on each fluid control volume, assuming the heat transfer at the fluid-solid boundary of the channel wall, Q_{loss}, was zero;

$$Q_{in} - Q_{loss} = \dot{m} C_p (T_{out} - T_{in}). \quad \text{eq (1)}$$

Q_{in} is constant and a function of the optical properties of the liquid and the radiative flux. These input parameters were then used to run the model in ANSYS. On convergence of the solution to a RMS residual error of 1×10^{-7}, the heat transfer at the fluid-solid boundary, Q_{loss}, is determined. A new bulk mean fluid temperature is then determined by accounting for the heat transfer through the fluid channel wall. This iterative procedure was repeated until the residual error in the temperature wall condition for both the hot and cold streams was less than 0.01^{0}C. Variations in the heat transfer coefficient due to changes in *Re* and *Pr* arising from the slight variation in the bulk mean fluid temperature between subsequent iterations was not considered.

Tab. 2 presents a summary of the fluid conditions considered in this study. For all inlet fluid temperatures considered the cooling stream flow was turbulent, however, the hot stream flow regime was highly dependent on the fluid temperature. Laminar, transitional and turbulent flow regimes were all covered. Convective heat transfer correlations for the hot channel and all external flows were based on hydraulic diameters. External wind velocities ranging from 2-10m/s were considered, which are typical of those encountered by NEP Solar's parabolic trough collectors during field operations. Reference dimension of the receiver are shown in Fig. 2 below.

Tab. 2 Flow Conditions

Parameter		Hot Fluid	Cooling Fluid
Fluid	-	Propylene Glycol	Water
Volume flow rate, $\dot{V}$	[L.min^{-1}]	5	2.5
Reynolds number, Re	-	69 – 3680	4595 – 9732
Prandtl number, Pr	-	16.2 – 700	2.98 – 7.01
Specific heat, c	[J.kg^{-1}.K^{-1}]	2458 – 3244	4183 – 4185
Thermal conductivity, k	[W.m^{-1}.K^{-1}]	0.19 – 0.2	0.60 – 0.65
Density, ρ	[kg.m^{-3}]	929 – 1037	983 – 998
Inlet temperature T_{in}	[°C]	20, 50, 80, 110, 130, 150	20, 40, 60
Ambient air temperature, T_∞	[°C]	15, 25, 35	
Air velocity, V_w	[m.s^{-1}]	2, 5, 10	

b. Heat Transfer Correlations for Fluid Streams

For fully developed turbulent flow conditions Nu was determined using the well-known Gnielinski correlation for forced convection in turbulent pipe flow (Gnielinski, 2010):

$$Nu_D = \frac{(f/8)RePr}{1 + 12.7(f/8)^{1/2}(Pr^{2/3} - 1)}\left[1 + (d_i/l)^{2/3}\right] \quad \text{eq (2)}$$

where f is the friction factor which can be determined, for smooth tubes, using the Konakov correlation; $f = (1.8 \log_{10} Re - 1.5)^{-2}$. Equation 2 is valid for $0.1 \leq Pr \leq 1000$ and $10^4 \leq Re \leq 10^6$.

For laminar flow entering the thermal receiver channel a boundary layer transformation must occur as the flow is split into two streams by the filter, which bisects the cylindrical tube. At this point the flow begins to be heated by the solar flux, assumed to be constant along the length of the receiver. For hydrodynamic and thermally developing laminar flow subject to constant heat flux equations suitable for all tube length can be obtained from

$$Nu_{m,q} = \left\{Nu_{m,q,1}^3 + 0.6^3 + \left(Nu_{m,q,2} - 0.6\right)^3 + Nu_{m,q,3}^3\right\}^{1/3} \quad \text{eq (3)}$$

where the asymptotes for the *mean Nusselt number* in a pipe of length l and internal diameter d_i are

$$Nu_{m,q,1} = 4.364 \quad \text{eq (4)}$$

for low values of $RePr\, d_i/l$ and

$$Nu_{m,q,2} = 1.953(RePr\, d_i/l)^{1/3} \quad \text{eq (5)}$$

for high values of $RePr\, d_i/l$. $Nu_{m,q,3}$ is a term used to adjust the correlation to account for the simultaneous hydrodynamic and thermal development and is expressed as

$$Nu_{m,q,3} = 0.924(Pr)^{1/3}(Re\, d_i/l)^{1/2}. \quad \text{eq (6)}$$

For flow in the transition region an interpolation method is used which applies an "intermittency factor" γ to account for the temporal sequences observed in the flow. Here $\gamma = 1$ if the flow is turbulent permanently and $\gamma = 0$ if the flow is permanently laminar. Using this approach Gnielinski proposed an equation to describe the Nusselt number correlation between permanent laminar and turbulent flow

$$Nu = (1-\gamma)Nu_{lam,2300} + \gamma Nu_{turb,10^4} \quad \text{eq (7)}$$

where γ is given by

$$\gamma = \frac{Re-2300}{10^4-2300}, \quad \text{and } 0 \le \gamma \le 1. \quad \text{eq (8)}$$

$Nu_{m,q,2300}$ is the Nusselt number at $Re = 2300$ calculated using equation 3, which can be expressed as

$$Nu_{m,q,2300} = \left\{83.326 + \left(Nu_{m,q,2,2300} - 0.6\right)^3 + Nu^3_{m,q,3,2300}\right\}^{1/3} \quad \text{eq (9)}$$

with

$$Nu_{m,q,2300} = 1.953(2300Pr\, d_i/l)^{1/3} \quad \text{eq (10)}$$

and

$$Nu_{m,q,3} = 0.924(Pr)^{1/3}(2300\, d_i/l)^{1/2}. \quad \text{eq (11)}$$

The fully developed turbulent Nusselt number correlation is determined from equation 1 at $Re = 10^4$

$$Nu_{m,10^4} = \frac{(0.0308/8)10^4 Pr}{1 + 12.7(0.0308/8)^{1/2}(Pr^{2/3}-1)}\left[1 + (d_i/l)^{2/3}\right] \quad \text{eq (12)}$$

External heat transfer coefficients accounted for heat loss via convection and radiation. To evaluate the influence of wind velocity on the heat transfer within the collector, forced convection heat transfer coefficients were estimated using heat transfer correlations for external flow across a tube (Zukauskas, 1972):

$$Nu_D = 0.683{Re_D}^{0.466}Pr^{1/3} \quad \text{for} \quad Re = 40 - 4{,}000$$

$$Nu_D = 0.193{Re_D}^{0.618}Pr^{1/3} \quad \text{for} \quad Re = 4{,}000 - 40{,}000. \quad \text{eq (13)}$$

The Reynolds number used for the glass tube surface was based on the external diameter, whereas the *Re* value for the outside of the rectangular insulation was based on a hydraulic diameter.

4. Results

Fig. 3 shows temperature contours within the receiver for thermal channel inlet temperature of $T_{hot,in} = 150$℃, cold channel inlet temperature $T_{cold,in} = 60$℃ and ambient air temperature $T_{\infty} = 15$℃. Heat conducted into the alanod mirrors is evident from the reduced wall temperatures in the region where the alanod meets the thermal channel. Although energy lost from the high temperature channel in this fashion is not collected in the form of high-grade heat, it is conducted through the alanod and aluminium extrusion and collected by the water in the cooling channel. The effects of this on the receiver efficiency are discussed in detail in section b. The temperature contours are presented here are typical in trend to those observed for all conditions.

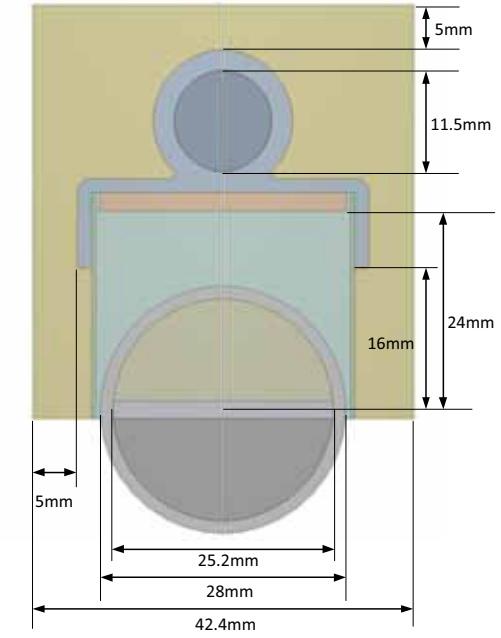

Fig. 2 Dimensions of hybrid receiver

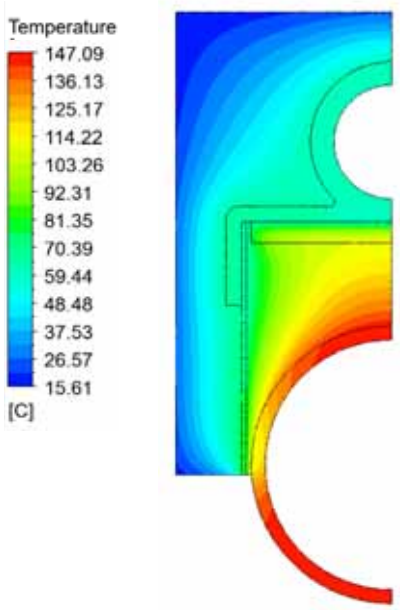

Fig. 3 Temperature contours for $\boldsymbol{T_{hot,in} = 150}$℃, $\boldsymbol{T_{cold,in} = 60}$℃, $\boldsymbol{T_{\infty} = 15}$℃

a. Variation of PV cell temperature

Fig. 4 below shows variations of average PV cell temperature, T_{PV}, plotted against hot channel bulk mean fluid temperature, $T_{f,h}$ for radiant flux values of 650 W/m^2 and 900 W/m^2. For the range of conditions modeled PV cell temperatures were between 40^{0}C and 92.5^{0}C. The temperature of the cell increases linearly with increasing cooling stream temperatures. This is an expected result given the low thermal resistance inherent between the silicon cells and the cooling stream. It can also be seen in Fig. 4 that the PV cell temperature increases linearly with the hot stream fluid temperature. However, the very gradual slope in the curve of T_{PV} versus $T_{f,h}$ indicates the effective decoupling of the PV cells from the hot fluid stream. For instance, a rise of 130^{0}C in the hot stream bulk fluid temperature (from 22^{0}C to 152^{0}C) results in a rise in the average PV cell temperature of 16^{0}C.

It should be noted that no contact resistance has been modeled between the PV cells and aluminium extrusion. The back-contact PV cells incorporate a complex electrode structure which would be expected to introduce contact resistance, which would increase the cell operating temperatures. Additionally, the electrical conversion efficiency of the silicon cells will fall with increasing temperature. This will in turn result in an increase in the heat generated within the cells, which would affect the linearity of the trends observed in Fig. 4.

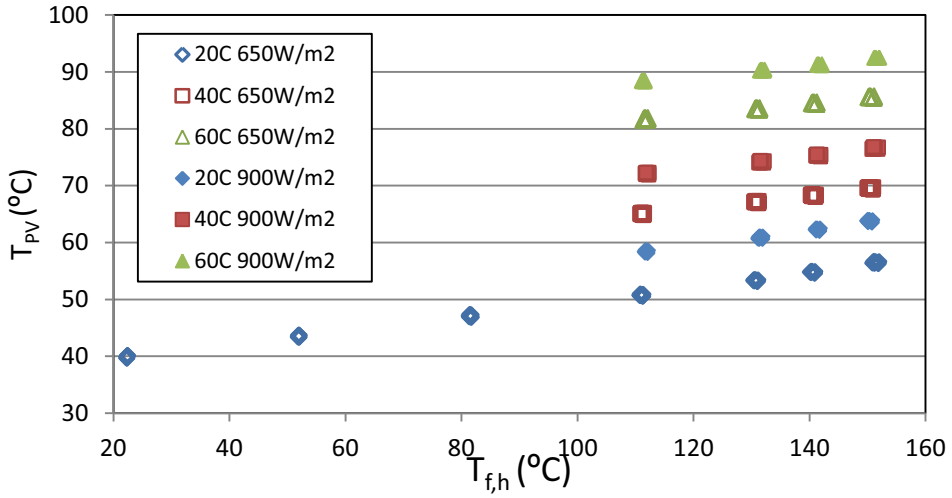

Fig. 4 Variation of average PV cell temperature with hot channel bulk mean fluid temperature

b. Hybrid Receiver Thermal Efficiency

Fig. 5, Fig. 6 and Fig. 7 present curves of hot channel thermal efficiency for cooling channel inlet temperatures of 20°C, 40°C and 60°C respectively. Here the efficiency is with respect to the fraction of energy which is ideally intended for absorption in the thermal receiver (see Tab. 1).

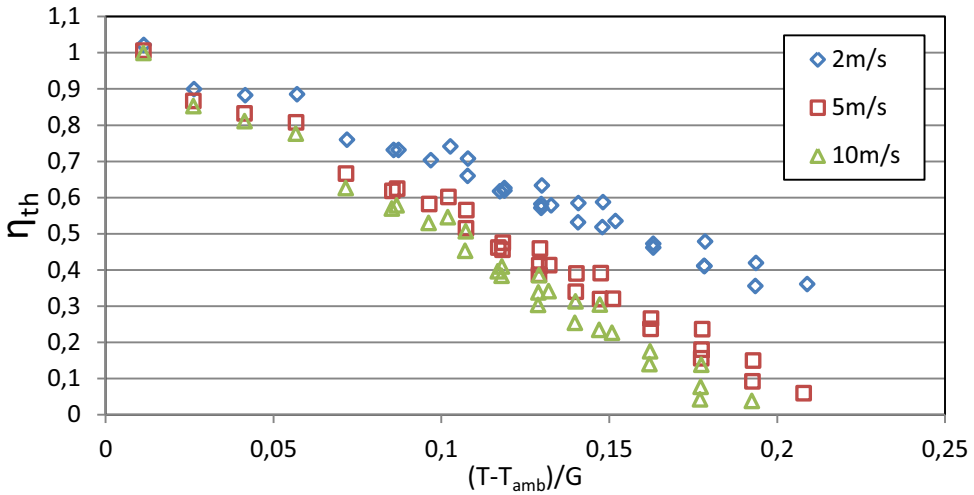

Fig. 5 Collector efficiency curve for $T_{cold,in}$ = 20°C

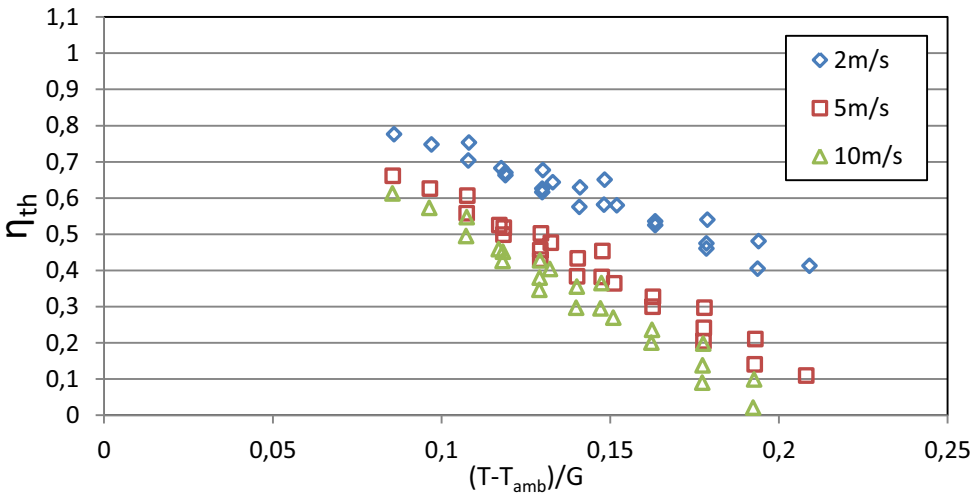

Fig. 6 Collector efficiency curve for $T_{cold,in}$ = 40°C

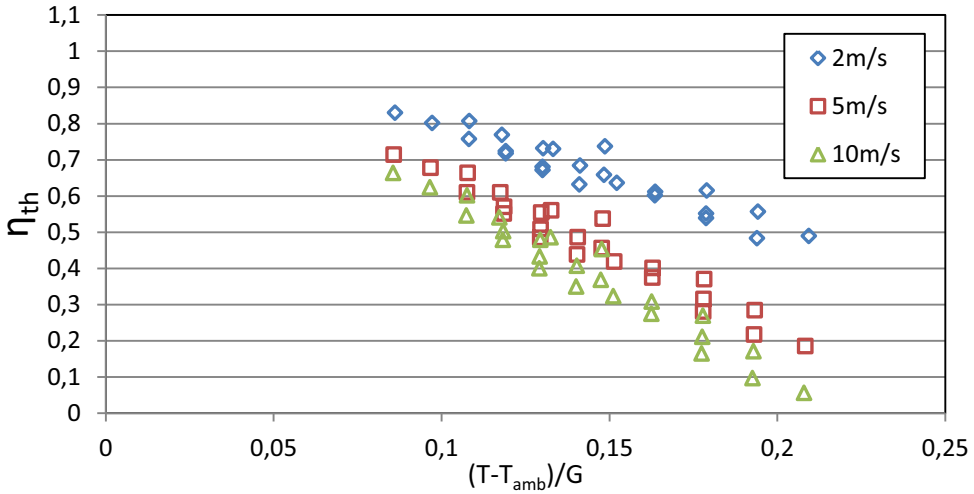

Fig. 7 Collector efficiency curve for $T_{cold,in} = 60$℃

It is immediately obvious that there is scatter in the efficiency curves, which is not typically expected in computational results. This scatter is caused by the strong influence of the convective heat loss from the glass thermal receiver tube with variations in ambient air temperature. To illustrate this point Fig. 8 shows the variation in thermal efficiency for a constant wind velocity of 2m/s and constant $T_{cold,in} = 20$℃.

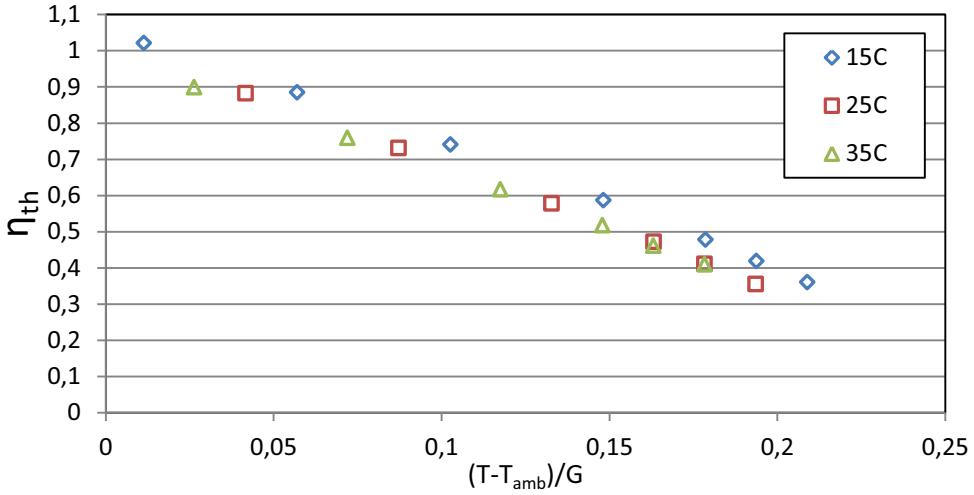

Fig. 8 Collector thermal efficiency for $T_{cold,in} = 60$℃, $V_{wind} = 2m/s$ for various T_{∞}

Additional to the thermal energy extracted from the hot stream, the beam splitting hybrid receiver also collects the dissipated energy within the PV cell in the cooling stream. Although this energy is low grade energy it can still be used for either domestic hot water or space heating. Fig. 9 shows an example of the energy extracted from the hot channel, the cooling channel and the PV cell for various hot stream bulk mean fluid temperatures, $T_{amb} = 25$℃, for a cooling channel inlet temperatures of $T_{cold,in} = 60$℃. It can be seen that as the bulk mean fluid temperature in the hot channel increases there is a reduction in the energy extracted by the hot stream. This is caused by the increased heat loss from the glass tube. However for the constant wind velocity and ambient air temperature conditions plotted in Fig. 9 the ratio of the heat loss to the ambient compared to the heat that is conducted towards the PV cells and cooling channel remains essentially constant. For this reason we see a corresponding gain in the heat energy collected in the cooling stream. Including the efficiency reduction in the PV cell with increase in temperature would affect this relationship. However, the overriding feature of the collector is that energy lost from the high temperature fluid stream is partially collected from the cooling stream.

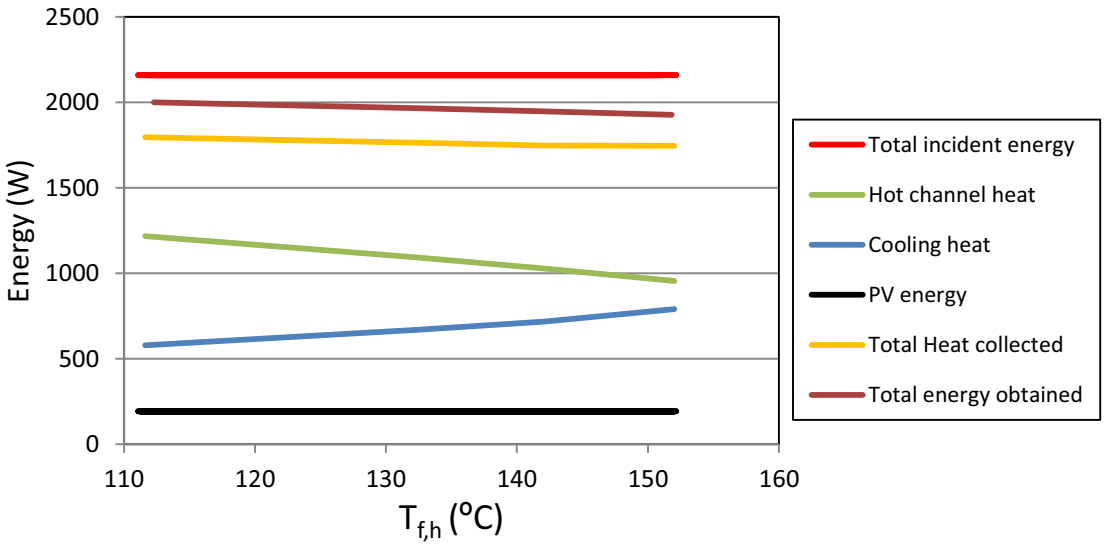

Fig. 9 Energy extraction from the hybrid receiver for G = 900 W/m^2, $T_{cold,in} = 60$℃, $V_{wind} = 2m/s$, and $T_{amb} = 25$℃

Numerous approaches have been used to report the overall system performance of PVT solar collectors. Some researchers have used the concept of a total system efficiency η_o, which is the direct sum of the thermal efficieny, η_{th} and the electrical efficiency, η_e (eg. Bhargava et al. (1991), Bergene and Løvvik (1995)). Other studies have scaled the electrical efficiency of the receiver using a power generation factor in an attempt account for the high-grade energy of the electricity output (eg. Tiwari et al. (2006), He et al. (2006)). Additionally exergy analyses are often used to evaluate the total energy conversion performance.

The primary objective of the current work was to investigate the thermal performance of the receiver, with particular attention on the high-grade thermal energy. Despite this, with reference to Fig. 9, it can be seen that applying the simplified total system approach referred to above, total system efficiencies in excess of 85% are capable. However, this value significantly under values the high grade thermal energy component of the collector. Future work will focus on addressing the limitations of this work, include the influence of PV efficiency temperature dependence and provide a thorough exergy analysis and provide an energy payback period assessment. Further to this the ability to tune the cut-off frequencies for the thermal absorber to customize the thermal and electrical outputs will also be addressed.

5. Conclusion

A hybrid beam splitting PVT collector has been designed for installation on linear concentrators, such as the NEP Solar Polytrough 1200. The high temperature heat exchange fluid, propylene glycol, volumetrically absorbs the long wavelength solar radiation (λ > 1100nm). A coloured filter contained within the propylene glycol acts as a high pass filter absorbing energy below λ < 700nm and transmitting the remainder of the spectrum to high efficiency, back contact silicon PV cells. A cooling channel on the back of the PV cells is designed to collect heat dissipated in the cells in the conventional PVT collector fashion.

Computational heat transfer modeling has been conducted on the receiver for a range of incident flux, fluid and ambient conditions. Results indicate the high temperature thermal outputs above 150°C are capable together with cooling channel outputs of 60°C. PV cell temperatures were shown to be increase linearly with both cooling channel and hot channel fluid temperature. However, for every degree in average PV cell temperature the hot channel was shown to increase approximately 8 °C. This indicates that the hot channel is effectively decoupled from the PV cells

Hot channel thermal efficiency was seen to be strongly correlated with the ambient wind velocity, as the high temperature walls of the thermal receiver tube are exposed to the wind. Despite this limitation, hot channel thermal efficiencies greater than 50% are capable, together with simplified system efficiencies of greater than 85%. These results demonstrate the hybrid beam splitting PVT receiver is a highly efficient solar energy solution with huge potential to meet building energy demands.

6. References

Bergene, T., Løvvik, O.M., 1995. Model calculations on a flat-plate solar heat collector with integrated solar cells. Solar energy 55, 453-462.

Bhargava, A.K., Garg, H., Agarwal, R.K., 1991. Study of a hybrid solar system—solar air heater combined with solar cells. Energy Conversion and Management 31, 471-479.

Chendo, M., Jacobson, M., Osborn, D., 1987. Liquid and thin-film filters for hybrid solar energy conversion systems. Solar & wind technology 4, 131-138.

Chow, T., He, W., Ji, J., 2006. Hybrid photovoltaic-thermosyphon water heating system for residential application. Solar energy 80, 298-306.

Dupeyrat, P., Ménézo, C., Rommel, M., Henning, H.-M., 2011. Efficient single glazed flat plate photovoltaic–thermal hybrid collector for domestic hot water system. Solar Energy 85, 1457-1468.

Fraisse, G., Ménézo, C., Johannes, K., 2007. Energy performance of water hybrid PV/T collectors applied to combisystems of Direct Solar Floor type. Solar Energy 81, 1426-1438.

Gnielinski, V., 2010. G1 Heat Transfer in Pipe Flow, VDI Heat Atlas. Springer Berlin Heidelberg, pp. 691-700.

He, W., Chow, T.-T., Ji, J., Lu, J., Pei, G., Chan, L.-s., 2006. Hybrid photovoltaic and thermal solar-collector designed for natural circulation of water. Applied Energy 83, 199-210.

Mojiri, A., Stanley, C., Rosengarten, G., 2014a. Quantifying the radiative flux distribution at the focal region of solar concentrators using digital photography, Solar 2014, Melbourne, Australia.

Mojiri, A., Stanley, C., Rosengarten, G., 2014b. Spectrally splitting hybrid photovoltaic/thermal receiver design for a linear concentrator. Energy Procedia In Press.

Peters, M., Goldschmidt, J.C., Löper, P., Groß, B., Üpping, J., Dimroth, F., Wehrspohn, R.B., Bläsi, B., 2010. Spectrally-selective photonic structures for PV applications. Energies 3, 171-193.

Tiwari, A., Sodha, M., Chandra, A., Joshi, J., 2006. Performance evaluation of photovoltaic thermal solar air collector for composite climate of India. Solar energy materials and solar cells 90, 175-189.

Zukauskas, A., 1972. Heat Transfer from Tubes in Crossflow. Advances in Heat Transfer 8, 93-106.